J. Fluid Mech. (1988), *vol.* 196, *pp.* 555–584
Printed in Great Britain

The turbulent near wake at a sharp trailing edge

By E. A. BOGUCZ† AND J. D. A. WALKER‡

† Department of Mechanical and Aerospace Engineering, Syracuse University, Syracuse, NY 13244, USA

‡ Department of Mechanical Engineering and Mechanics, Lehigh University, Bethlehem, PA 18015, USA

(Received 1 June 1987 and in revised form 13 June 1988)

The problem of a turbulent boundary layer that evolves into a wake flow at the sharp trailing edge of a thin flat plate is considered; the formal structure of the near-wake flow is investigated using matched expansions in the limit of infinite Reynolds number. The symmetric turbulent near wake is shown to develop a two-layer structure which is independent of turbulence model. The general asymptotic analysis shows that a thin layer at the wake centreline grows linearly with distance from the trailing edge while the centreline velocity varies logarithmically in a manner that is supported strongly by experimental measurements. The relatively thick outer layer of the near-wake flow is undisturbed by the evolution of the inner layer to leading order. An additional region near the trailing edge is required to resolve a non-uniformity in transverse velocity. The general asymptotic results are used to guide the development of a zonal turbulence model for the near wake in the form of a simple eddy viscosity formula. Analytic profiles for velocity and Reynolds stress are obtained for the near-wake region; these profiles are shown to provide accurate representations of available near-wake experimental data.

1. Introduction

The flow that develops in the near wake of a surface as a boundary layer leaves a sharp trailing edge is a fundamental problem of considerable theoretical and practical significance. In particular, the effects of trailing-edge flows are recognized to be potentially significant in the design of airfoils as well as turbine and compressor blades; it is therefore of interest to develop methods for the accurate prediction of such situations. From a theoretical standpoint, the near-wake problem for a flat plate is the simplest situation at a trailing edge and here an abrupt change in boundary conditions occurs from the no-slip condition on the surface to a symmetry condition in the near wake. If the surface boundary layer is laminar, the formal structure of the flow field is well understood; the near-wake flow is described by the Goldstein (1930) solution and between this region and the upstream boundary layer, a triple-deck structure occurs (Stewartson 1969; Messiter 1970). It emerges that the laminar triple deck appears in a wide variety of other physical situations and subsequent studies led to major advances in the analysis of such problems as viscous–inviscid interactions, boundary-layer separation and internal flows (see, for example, Stewartson 1974; Smith 1982). A complete description for turbulent trailing-edge flows has yet to be established; the present study is intended to contribute to a more complete understanding of the situation when the surface boundary-layer flow is turbulent.

The mathematical problem considered here is that of a turbulent flow at a trailing edge of a thin flat plate that is aligned parallel to a constant-pressure, uniform mainstream. A principal objective of this study is to describe the formal structure of the flow downstream of the trailing edge and results that are independent of the turbulence model (used to close the governing equations) are of principal interest. To achieve this end, the method of matched expansions and singular perturbation theory are used to identify the different regions of the flow field in the limit of infinite Reynolds number. The asymptotic analysis is carried out prior to the adoption of a specific turbulence model and the approach is similar to the previous general analyses of Mellor (1972) and Fendell (1972) for attached turbulent boundary-layer flows.

In the present work, some of the partial results obtained in previous studies are generalized and extended. A detailed critical review of previous theoretical investigations of turbulent trailing-edge flows has been given by Bogucz (1984) and only a brief summary is included here. Robinson (1969) considered the turbulent near-wake flow problem in an analysis based on previous work by Townsend (1965, 1966) associated with determining the response of a turbulent boundary layer to an abrupt change in surface roughness. Townsend (1965, 1966) showed that the bulk of the boundary layer is slow to respond to the change at the surface and that most of the streamwise velocity profile persists for relatively long distances downstream of the modification. A similar behaviour occurs at a sharp trailing edge and Robinson (1969) was able to show that the major changes in the profile occur in a region near the wake centreline; using an informal analysis, he obtained a self-similar solution for this region that included a logarithmic dependence in the centreline velocity. More recently, Alber (1980) has proposed a detailed structure for the wake flow of a plate in which the wake is divided into a number of regions. A specific turbulence model is adopted at the outset of the analysis and Alber (1980) obtains solutions for some portions of the near-wake flow that exhibit a logarithmic dependence on centreline velocity. However, Alber's (1980) adduced structure is based largely on intuitive arguments, some of which are questionable. For example, a region immediately downstream of the trailing edge on the wake centreline was proposed where the flow is assumed to be governed by the laminar boundary-layer equations. In addition, the extent of the dependence of the reported results on the intuitive reasoning and the adopted turbulence model is not clear; in fact, the turbulence model leads to a velocity profile in the near wake that has a non-vanishing velocity gradient on the wake centreline and this is not physically realistic. Prabhu & Patel (1982) also rely on a specific closure assumption to consider the near-wake flow problem, although the model is somewhat more general than that used by Alber (1980). An asymptotic analysis based entirely on the Cebeci & Smith (1974) turbulence model applied to the prediction of the turbulent boundary layer on a finite flat plate has been reported recently by Neish & Smith (1988), who also consider the development of the downstream wake flow using the Cebeci–Smith scheme. The suitability of the Cebeci–Smith model for wake calculations will be discussed subsequently, at which point further comment will be made regarding the wake results of Neish & Smith (1988).

It is worth noting that a series of trailing-edge problems have been successfully analysed using asymptotic methods. These studies include flow at the cusped trailing edge of a plate aligned at angle of attack to the mainstream flow (Melnik & Chow 1975; Melnik, Chow & Mead 1977; Melnik 1980) and the flow at a wedge-shaped trailing edge (Melnik & Grossman 1981). In these situations, it has been demonstrated that the turbulent boundary layer develops a three-layer structure near the trailing

edge; however, such trailing-edge flows are dominated by the presence of singularities in the leading-order external flow solution, which is not the case in the present problem.

The asymptotic theory employed in the first part of this study leads to a general description of the flow structure at the trailing edge that is independent of turbulence model. However in order to produce a solution for the velocity and Reynolds stress profiles in the near-wake region, it is necessary to adopt a model for the Reynolds stresses that appear in the time-mean equations. In the near-wake region, the simplest possible eddy viscosity model was used to produce closure; the results of the asymptotic theory were used to guide the selection of this model.

The plan of the paper is as follows. In §2, the structure of the flow upstream of the trailing edge is reviewed. The asymptotic analysis of the near-wake flow is presented in §3, and the principal results are discussed in §4. Suitable turbulence models for closure of the near-wake governing equations are presented in §5, and in §6, computed near-wake results are compared with experimental measurements. The principal results of the study are summarized in §7.

2. The surface boundary layer

Consider a flat plate of length L that is immersed in an incompressible fluid of density ρ and absolute viscosity μ; a flow of speed U_0 moves in a direction parallel to the plate surface. A Blasius boundary-layer flow develops in a direction downstream from the leading edge but when the Reynolds number, $Re = \rho U_0 L/\mu$, is sufficiently large, transition to a fully turbulent boundary-layer flow occurs on the latter portion of the plate surface. In this study, the surface boundary layer approaching the trailing edge is assumed to be fully turbulent and nominally steady. The equations governing the time-mean flow field are taken to be the Reynolds equations; in dimensionless form, the two-dimensional Navier–Stokes equations are

$$\left.\begin{aligned} \frac{\partial \bar{u}}{\partial x}+\frac{\partial \bar{v}}{\partial y} &= 0, \\ \bar{u}\frac{\partial \bar{u}}{\partial x}+\bar{v}\frac{\partial \bar{u}}{\partial y} &= -\frac{\partial \bar{p}}{\partial x}+\frac{1}{Re}\left[\frac{\partial^2 \bar{u}}{\partial x^2}+\frac{\partial^2 \bar{u}}{\partial y^2}\right]-\frac{\partial \overline{u'^2}}{\partial x}-\frac{\partial \overline{u'v'}}{\partial y}, \\ \bar{u}\frac{\partial \bar{v}}{\partial x}+\bar{v}\frac{\partial \bar{v}}{\partial y} &= -\frac{\partial \bar{p}}{\partial y}+\frac{1}{Re}\left[\frac{\partial^2 \bar{v}}{\partial x^2}+\frac{\partial^2 \bar{v}}{\partial y^2}\right]-\frac{\partial \overline{u'v'}}{\partial x}-\frac{\partial \overline{v'^2}}{\partial y}. \end{aligned}\right\} \tag{2.1}$$

Here x and y are Cartesian coordinates with corresponding mean velocity components $\bar{u}$ and $\bar{v}$; the plate coincides with the x-axis and the origin is located at the trailing edge. On the plate surface, the boundary-layer flow must satisfy the boundary conditions

$$\bar{u} = \bar{v} = 0 \quad \text{at } y = 0; \qquad \bar{u} \to 1 \quad \text{as } y \to \infty, \tag{2.2}$$

and any models for the turbulence terms must satisfy

$$\overline{u'^2} = \overline{v'^2} = \overline{u'v'} = 0 \quad \text{at } y = 0 \quad \text{and as } y \to \infty. \tag{2.3}$$

Although the asymptotic structure of a fully turbulent boundary-layer flow is well known (cf. Fendell 1972; Mellor 1972), a brief review of the principal features is necessary to establish the basis of the subsequent near-wake analysis.

The turbulent boundary layer is a composite double layer and an important small

parameter that arises in the asymptotic analysis in the limit $Re \to \infty$ (Fendell 1972) is the friction velocity

$$u_*(x; Re) = (\tau_w(x; Re))^{\frac{1}{2}}, \tag{2.4}$$

where τ_w is the local non-dimensional wall shear stress. In the outer layer, the streamwise velocity is in the form of a defect law and the Reynolds stress is $O(u_*^2)$, viz.

$$\bar{u} = 1 + u_* \frac{\partial F_1}{\partial \eta}(x, \eta) + \ldots, \quad -\overline{u'v'} = u_*^2 \Sigma_1(x, \eta) + \ldots. \tag{2.5}$$

In (2.5), η is the scaled outer-layer variable $\eta = y/\Delta_0(x; Re)$, where Δ_0 is a quantity proportional to the local boundary-layer thickness, and Σ_1 is a function that must be specified to define a particular turbulence model. The outer-layer lengthscale Δ_0 is $O(u_*)$ (Fendell 1972); however, if δ^* denotes the local (non-dimensional) displacement thickness, it follows (upon neglecting the contribution due to the wall layer) that

$$\delta^* = \int_0^\infty (1 - \bar{u})\, dy = -\Delta_0 u_* \lim_{\eta \to \infty} F_1(x, \eta) + \ldots, \tag{2.6}$$

and consequently a convenient choice is

$$\Delta_0 = \frac{\delta^*}{u_*}, \quad \lim_{\eta \to \infty} F_1(x, \eta) = -1. \tag{2.7}$$

It may than be shown that the leading-order form of the x-momentum equation in the outer layer is

$$\frac{\delta^*}{u_*^2} \frac{\partial^2 F_1}{\partial x \partial \eta} - \eta \frac{\partial^2 F_1}{\partial \eta^2} = \frac{\partial \Sigma_1}{\partial \eta}, \tag{2.8}$$

and the corresponding transverse velocity is

$$\bar{v} = u_*^2 \left[\eta \frac{\partial F_1}{\partial \eta} - F_1 \right] - \delta^* \frac{\partial F_1}{\partial x}. \tag{2.9}$$

The outer-layer velocity expansion in (2.5) is not uniformly valid and in order to satisfy the no-slip condition, a thin inner wall layer is required; in this region, the convective terms are negligible to leading order (Fendell 1972) and the expansions are of the form

$$\bar{u} = u_* U^+(y^+) + \ldots, \quad -\overline{u'v'} = u_*^2 \sigma_1(y^+) + \ldots. \tag{2.10}$$

Here, y^+ is the scaled inner coordinate defined by

$$y^+ = \frac{y}{\Delta_i}, \quad \Delta_i = \frac{1}{Re\, u_*}, \tag{2.11}$$

and U^+ and σ_1 can be shown to satisfy

$$U^{+\prime\prime} + \sigma_1' = 0. \tag{2.12}$$

Note that σ_1 is a function that must be specified to define a particular turbulence model.

Matching of the expansions (2.5) and (2.10) takes place in the limits $\eta \to 0$ and $y^+ \to \infty$ and a self-consistent structure can be obtained for

$$\frac{\partial F_1}{\partial \eta} \sim \frac{1}{\kappa} \log \eta + C_0, \quad \Sigma_1 \sim 1 + \ldots \quad \text{as } \eta \to 0, \tag{2.13}$$

$$U^+ \sim \frac{1}{\kappa} \log y^+ + C_i, \quad \sigma_1 \sim 1 + \ldots \quad \text{as } y^+ \to \infty. \tag{2.14}$$

In (2.13) and (2.14), κ is the von Kármán constant and C_i is the inner 'log-law' constant, which are commonly assumed to have universal values of $\kappa = 0.41$ and $C_i = 5.0$; C_o, the outer 'log-law' constant, varies with x in general and depends on the specific outer-region turbulence model. The matching process produces a fundamental relation between scales, namely

$$\frac{1}{u_*} = \frac{1}{\kappa}\log(u_* \Delta_o Re) + C_i - C_o, \tag{2.15}$$

which will be referred to as the match condition; this relation is often called the 'skin friction relation' and is well supported by experimental data (Rotta 1962).

In the present configuration, the boundary-layer flow will approach a condition of self-similarity near the trailing edge provided the plate is long enough. Defining ϵ by

$$\epsilon = \lim_{x \to 0^-} u_*(x; Re), \tag{2.16}$$

the expansions (2.5) and (2.9) near the trailing edge become

$$\bar{u} = 1 + \epsilon F_1'(\eta) + \ldots, \quad \bar{v} = \epsilon^2(\eta F_1'' - F_1) + \ldots, \quad -\overline{u'v'} = \epsilon^2 \Sigma_1(\eta) + \ldots. \tag{2.17}$$

Here the primes denote differentiation with respect to η and (2.8) becomes

$$-\eta F_1'' = \Sigma_1'. \tag{2.18}$$

Using (2.13) and the conditions

$$F_1', \Sigma_1 \to 0 \quad \text{as } \eta \to \infty, \tag{2.19}$$

a useful first integral of (2.18) may be obtained according to

$$F_1 - \eta F_1' = \Sigma_1 - 1. \tag{2.20}$$

It should be noted that the results in this section are general and may be derived independently of specific turbulence modelling considerations; however, in order to obtain solutions for the velocity and Reynolds stress profiles, specification of turbulence models for the inner and outer layers is ultimately required. Suitable turbulence models are discussed in §5.

3. The near-wake region

3.1. *Introduction*

As the turbulent boundary layer leaves the plate surface, the flow must adjust to the abrupt change in boundary conditions. On the plate surface, the streamwise velocity satisfies the no-slip condition; in the wake, the $\bar{u}$ velocity profile must satisfy the symmetry condition of zero shear on the wake centreline and here strong acceleration is expected as a consequence of the sudden removal of the no-slip condition. In this section the asymptotic structure of the near-wake region in the limit $Re \to \infty$ is described. The analysis is carried out generally without specifying a particular closure scheme for the unknown Reynolds stress terms; indeed, the theoretical development indicates that conventional closure schemes which are typically used for wall boundary layers are inappropriate for the near-wake flow. The present theory indicates the form required for near-wake flows and suitable models are ultimately developed in §5.

The basic flow structure is depicted schematically in figure 1. The flow in the outer

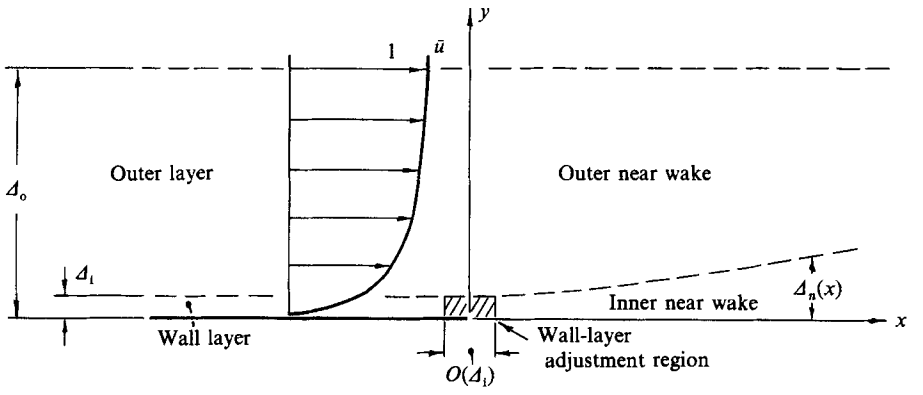

FIGURE 1. Near-wake flow geometry.

layer of the surface boundary layer passes into an 'outer-near-wake' region almost as if unaware of the disappearance of the plate. A thin 'inner-wake' region develops at the wake centreline and it is here that the primary effects of the change in boundary conditions at the trailing edge occur. As the flow evolves into the near wake, the outer-wake region is subject to perturbations induced by the accelerating flow in the inner wake. A third region that will be discussed in the subsequent presentation is an adjustment zone that is required to resolve a non-uniformity in the transverse velocity which arises in the outer layers of the trailing-edge flow. The wake structure is partially determined by requiring that the near-wake structure match the surface boundary-layer solution in the limit $x \to 0^+$. In the subsequent analysis, the parameter ϵ denotes the limit of the skin friction velocity as $x \to 0^-$, defined by (2.16); in addition, the surface boundary-layer scales Δ_0 and Δ_i are taken to be constants equal to their values at the trailing edge in the limit $x \to 0^-$.

3.2. *The inner near wake*

The near-wake analysis begins by consideration of a thin region along the wake centreline having a thickness proportional to $\Delta_n(x; Re)$ as indicated in figure 1. At the outset, the thickness Δ_n is unknown but is assumed to be formally bounded by the lengthscales of the surface boundary layer; in the inner wake, a scaled normal variable z is defined by

$$z = \frac{y}{\Delta_n(x; Re)}, \quad \Delta_i \ll \Delta_n \ll \Delta_0. \tag{3.1}$$

In order for the flow in the inner near wake to match the continuation of the outer-layer surface profile, it follows from (2.13) and (2.17) that

$$\bar{u} \sim 1 + \epsilon\left[\frac{1}{\kappa}\log\left(\frac{\Delta_n}{\Delta_0}\right) + \frac{1}{\kappa}\log z + C_0\right] + \ldots \quad \text{as } z \to \infty, \tag{3.2}$$

for small positive x. This equation suggests that the streamwise velocity in the inner near wake should be written in the form

$$\bar{u} = u_c(x; Re) + \epsilon\frac{\partial f}{\partial z} + \ldots. \tag{3.3}$$

Here u_c is the leading-order approximation to the centreline velocity which is to be determined; in addition $f = f(x, z)$ in general and with $u_c \gg \epsilon$, $\epsilon\partial f/\partial z$ represents the leading-order perturbation to the centreline velocity in the near wake. The

corresponding form of the transverse velocity follows from the continuity equation in (2.1), viz.

$$\bar{v} = -\Delta_n u_c' z - \epsilon \Delta_n \frac{\partial f}{\partial x} + \epsilon \Delta_n' \left(z \frac{\partial f}{\partial z} - f \right) + \ldots, \tag{3.4}$$

where the prime denotes differentiation with respect to x. Finally, the pressure and Reynolds stress in the inner near wake are written according to

$$\bar{p} = p_0 + \epsilon^2 p_1(x,z) + \ldots, \quad -\overline{u'v'} = \epsilon^2 \sigma(x,z) + \ldots. \tag{3.5a,b}$$

Here p_0 is the constant mainstream pressure and p_1 is a perturbation term due to the displacement-thickness effect of the turbulent boundary layer on the plate surface. Note that (3.5*b*) is simply a statement that the Reynolds stress in the inner near wake has the same order of magnitude as in the surface boundary layer. To leading order, the Reynolds stress in the outer layer continues unaltered into the outer near wake and, in order for σ to match the outer-near-wake Reynolds stress, it follows that

$$\sigma \sim 1 \quad \text{as } z \to \infty. \tag{3.6}$$

Apart from condition (3.6), the function σ is taken to be an arbitrary function in this section since the principal interest is in obtaining results that are independent of an imposed turbulence model; the analysis does however suggest an appropriate form for σ in the near wake.

It is assumed that $\overline{u'^2}$ in the near wake is of the same order of magnitude as in the surface boundary layer (i.e. $O(\epsilon^2)$) and upon substitution of (3.3)–(3.5) in (2.1), the leading-order terms in the streamwise momentum equation are

$$\frac{\Delta_n u_c}{\epsilon} \frac{\partial^2 f}{\partial x \partial z} + \frac{\Delta_n u_c u_c'}{\epsilon^2} - \frac{\Delta_n' u_c}{\epsilon} z \frac{\partial^2 f}{\partial z^2} + \frac{\Delta_n u_c'}{\epsilon} \left[\frac{\partial f}{\partial z} - z \frac{\partial^2 f}{\partial z^2} \right] = \frac{\partial \sigma}{\partial z}. \tag{3.7}$$

The omitted terms in (3.7) are $O(\Delta_n)$ and $O(\Delta_n')$. The absence of a lengthscale suggests a similarity solution may be available and this is possible if the second term and the coefficient of the third term are independent of x. For this to occur, it is evident that u_c must be logarithmic in Δ_n; the form consistent with condition (3.2) at the outer edge of the near wake is

$$u_c(x; Re) = 1 + \frac{\epsilon}{\kappa} \log \left(\frac{\Delta_n}{\Delta_0} \right). \tag{3.8}$$

For convenience (and without loss of generality) the coefficient of the third term in (3.7) is taken equal to κ, the von Kármán constant, and this (in conjunction with (3.8)) provides the defining relation for the inner scale Δ_n, viz.

$$\frac{\Delta_n'}{\epsilon} \left[1 + \frac{\epsilon}{\kappa} \log \frac{\Delta_n}{\Delta_0} \right] = \kappa. \tag{3.9}$$

This equation may be integrated to yield

$$\Delta_n \left[1 + \epsilon \left(\frac{1}{\kappa} \log \frac{\Delta_n}{\Delta_0} - \frac{1}{\kappa} \right) \right] = \epsilon \kappa [x - x_0], \tag{3.10}$$

where x_0 is a constant of integration. It is easily verified that $\Delta_n = O(\Delta_i)$ as $x \to 0^+$ for Re fixed and large, and it is convenient to take $\Delta_n = \Delta_i$ in this limit which defines the constant x_0 according to

$$x_0 = -\frac{1}{\kappa} \left(C_i - C_0 - \frac{1}{\kappa} \right) \Delta_i. \tag{3.11}$$

Note that for $x \gg \Delta_i$, x_0 in (3.10) is negligible.

With u_c and Δ_n defined by (3.8) and (3.10) respectively it follows that

$$\frac{\Delta_n u_c u_c'}{\epsilon^2} = 1, \quad \frac{\Delta_n' u_c}{\epsilon} = \kappa; \tag{3.12}$$

furthermore the last term on the left-hand side of (3.17) is $O(\Delta_n')$ and therefore negligible. It is worth noting that a meaningful description of the inner near-wake flow requires that both the second and third terms in (3.7) enter the leading-order equation. The third term must be $O(1)$ if the leading-order equation is to describe a non-trivial flow in the inner near wake; the second term is required to be $O(1)$ in order that the inner-wake equation contains a new feature not present in the surface outer-layer description, namely the expected intense streamwise variation of $u_c(x; Re)$ in the near wake. With the leading terms in the near-wake region given by a similarity solution according to

$$f(x,z) = f_w(z) + \ldots, \quad \sigma(x,z) = \sigma_w(z) + \ldots, \tag{3.13}$$

it is easily shown from (3.7) that

$$1 - \kappa z f_w'' = \sigma_w'. \tag{3.14}$$

Here the prime denotes differentiation with respect to z. The boundary conditions for f_w and the Reynolds stress function are

$$f_w(0) = f_w''(0) = \sigma_w(0) = 0, \tag{3.15}$$

on the wake centreline and

$$f_w' \to \frac{1}{\kappa}\log z + C_0, \quad \sigma_w \to 1 \quad \text{as } z \to \infty, \tag{3.16}$$

to match the continuation of the surface outer layer into the near wake. A useful first integral of (3.14) may be obtained by integrating from the wake centreline and using (3.15). It follows that

$$z - \kappa(z f_w' - f_w) = \sigma_w. \tag{3.17}$$

The general asymptotic form of f_w at the outer edge of the inner near wake follows from (3.16) and (3.17), viz.

$$f_w \sim \frac{z}{\kappa}\left(\log z - 1 + \kappa C_0\right) + \frac{1}{\kappa} \quad \text{as } z \to \infty. \tag{3.18}$$

To obtain further details concerning the velocity distribution in the inner near wake, it is necessary to specify a particular turbulence model for σ_w and this aspect is considered in §5.

The inner lengthscale Δ_n, defined by (3.10), is a fundamental and general result of the analysis; some significant features of Δ_n warrant further discussion. In particular, in the limit $Re \to \infty$, is easily shown from (3.10) that for fixed x

$$\Delta_n \sim \epsilon\kappa x\left[1 - \frac{\epsilon}{\kappa}\left(\log\frac{\kappa x}{\Delta_0/\epsilon} - 1\right) + \ldots\right] \tag{3.19}$$

(note that $\epsilon \to 0$ in the limit $Re \to \infty$, and Δ_0 is $O(\epsilon)$). It is evident that, to leading order, the thickness of the inner near wake grows linearly with distance from the trailing edge. The behaviour of the ratio Δ_n/ϵ given by (3.10) is depicted in figure 2 for several values of ϵ, along with the limiting behaviour $\Delta_n/\epsilon \sim \kappa x$ (the conventional values $\kappa = 0.41$, $C_i = 5.0$, and $C_0 = 0.979$ have been used in preparing this figure). Note that for values of ϵ typically encountered in practice ($\epsilon \approx 0.04$), many terms in the

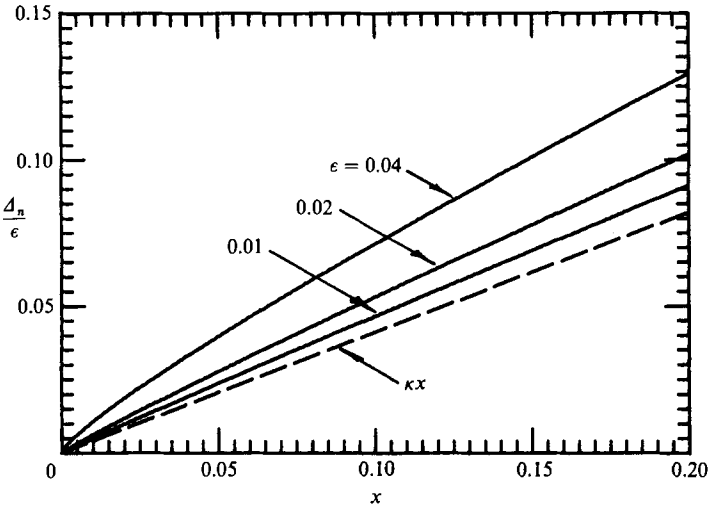

FIGURE 2. Development of scaled inner-wake thickness, Δ_n/ϵ.

expansion (3.19) would be required to obtain an accurate evaluation of Δ_n. While (3.19) describes the behaviour of Δ_n at fixed x in the limit $Re \to \infty$, an alternative expression of (3.10) is appropriate for distances from the trailing edge comparable with the surface wall-layer thickness. Using (2.15), equation (3.10) may be rewritten

$$\frac{\Delta_n}{\Delta_i}\left[\frac{1}{\kappa}\log\frac{\Delta_n}{\Delta_i} - \kappa\frac{x_0}{\Delta_i}\right] = \kappa\frac{x-x_0}{\Delta_i}, \tag{3.20}$$

where here x_0 is given by (3.11). It follows that in the limit $x \to 0$, $Re \to \infty$ with x/Δ_i fixed, Δ_n is $O(\Delta_i)$.

The relations that have been obtained for the inner-wake velocity and lengthscales may be used to evaluate the range of validity of the present analysis. It is easily confirmed using (2.15) and (3.8) that $u_c \gg \epsilon$ where $\Delta_n \gg \Delta_i$ and vice versa. On the other hand, (3.20) shows that Δ_n is $O(\Delta_i)$ when $x = O(\Delta_i)$; consequently the assumptions of the analysis are violated when $x = O(\Delta_i)$ and it is necessary to introduce a new subregion $O(\Delta_i) \times O(\Delta_i)$ centred at the trailing edge. This subregion is shown schematically in figure 1; the zone contains the response of the surface wall layer to the change in boundary conditions at $x = 0$ and here both $\bar{u}$ and $\bar{v}$ are $O(\epsilon)$. In addition, all three Reynolds stress terms $\overline{u'^2}$, $\overline{u'v'}$ and $\overline{v'^2}$, which are $O(\epsilon^2)$, enter the momentum equations (2.1) to leading order; thus it is necessary to model three turbulence functions in order to obtain solutions in this region. However in the limit $Re \to \infty$, the region is transcendentally small and since it does not appear to be significant in the leading-order description of the trailing-edge flow, it will not be considered further.

A significant general result of the inner-wake analysis concerns the behaviour of the transverse velocity as $z \to \infty$ which determines the influence of the inner wake on the outer portion of the wake shear layer. It follows from (3.4), (3.12), (3.13) and (3.18) that

$$\bar{v} \sim -\frac{\epsilon}{\kappa}\Delta_n' + \ldots \quad \text{as } z \to \infty. \tag{3.21}$$

Since $\Delta_n' > 0$, (3.21) describes a continual inflow into the inner wake from the outer wake; this is the behaviour that is expected on physical grounds to allow for an

acceleration of the streamwise velocity along the wake centreline. It is worth noting that, from (3.8), (3.9) and (3.21), the transverse velocity into the inner wake is $O(\epsilon^2/u_c)$; thus as $x \to 0^+$, $\bar{v}$ is eventually $O(\epsilon)$ in the vicinity of the square region $O(\Delta_i)$ near the trailing edge. The negative transverse velocity into the inner near wake is in contrast to the surface boundary layer where $\bar{v}$ is everywhere positive. The rest of the flow field must adjust to the negative $\bar{v}$ in the inner wake, and the outer near-wake region is considered next.

3.3. *The outer near wake*

As the outer-layer surface flow evolves into the near wake, the streamwise velocity and Reynolds stress distributions are essentially preserved but the transverse velocity must respond to the inflow to the inner wake. The form of the expansion for $\bar{v}$ is suggested by (3.21) and in the outer near wake, the velocity components and Reynolds stress are written to leading order according to

$$\bar{u} = 1 + \epsilon F_1'(\eta) + \epsilon x \frac{\epsilon}{\Delta_0} F_w'(\eta) + \ldots, \tag{3.22}$$

$$\bar{v} = -\frac{\epsilon}{\kappa} \Delta_n' - \epsilon^2 F_w(\eta) + \ldots, \tag{3.23}$$

$$-\overline{u'v'} = \epsilon^2 \Sigma_1(\eta) + \ldots. \tag{3.24}$$

Here $F_1(\eta)$ and $\Sigma_1(\eta)$ are the velocity profile and Reynolds stress functions in the outer layer of the surface boundary layer evaluated as $x \to 0^-$; the function $F_w(\eta)$ is a wake profile function which is to be determined subject to the condition

$$F_w(0) = 0. \tag{3.25}$$

It is easily verified that the expansions (3.22)–(3.24) match the upstream boundary-layer solutions as $x \to 0^+$ and the inner near-wake solutions as $\eta \to 0$ for fixed x. Substitution into (2.1) shows that the Reynolds stress gradient and the streamwise convection term are the dominant terms in the streamwise momentum equation and the leading-order equation is

$$F_w' = \Sigma_1'. \tag{3.26}$$

Since $\Sigma_1 \to 1$ as $\eta \to 0$, it follows from (3.25) that

$$F_w(\eta) = \Sigma_1(\eta) - 1. \tag{3.27}$$

The outer-wake function may also be expressed in terms of the surface boundary-layer profile $F_1(\eta)$ through (2.8); for a self-similar boundary layer at the trailing edge, (2.20) shows that

$$F_w(\eta) = F_1(\eta) - \eta F_1'(\eta). \tag{3.28}$$

Since $F_1' \to 0$ as $\eta \to \infty$, it may be seen using (2.7) that the asymptotic forms of F_w are

$$F_w \to -1, \quad F_w' \to 0 \quad \text{as } \eta \to \infty. \tag{3.29}$$

In addition, for small η,

$$F_w \sim -\frac{\eta}{\kappa} \quad \text{as } \eta \to 0, \tag{3.30}$$

and it may be confirmed from (3.22) that the outer-wake function F_w gives rise to a small deceleration at the outer edge of the inner near wake.

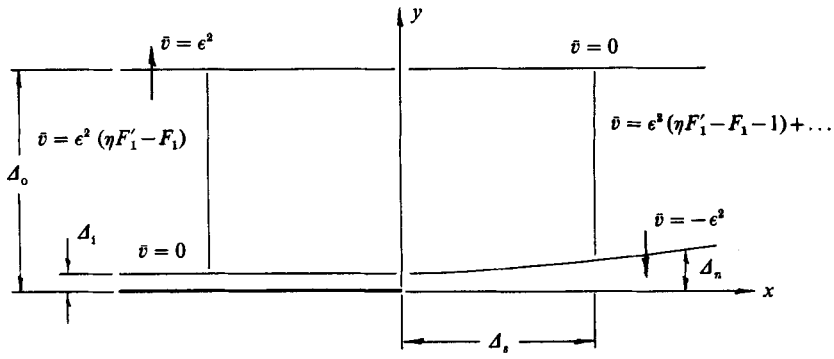

FIGURE 3. Non-uniformity in outer-layer transverse velocity.

It is worth noting that it may be easily shown, using the results of §2, that the leading term for $\partial\bar{u}/\partial x$ in the outer layer of the surface boundary layer is

$$\frac{\partial \bar{u}}{\partial x} = \frac{u_*^2}{\Delta_0} \frac{\partial \Sigma_1}{\partial \eta}, \tag{3.31}$$

at any $x \leqslant 0$. Consequently, in view of (3.26), the expansion in (3.22) represents the first two terms in a Taylor series expansion of $\bar{u}$ for fixed y evaluated as $x \to 0^-$, and (3.22) is simply the analytic continuation of the outer-layer surface profile into the wake.

3.4. *Trailing-edge adjustment region*

The leading-order near-wake solution described thus far is valid for x small and $O(1)$; however the description is not uniformly valid as $x \to 0$. One non-uniformity in the inner near-wake solution, associated with a transcendentally small region (as $Re \to \infty$) $O(\Delta_1) \times O(\Delta_1)$ near the trailing edge, has previously been discussed. An additional non-uniformity occurs in the outer-wake region as a consequence of the behaviour of the transverse velocity. On the plate surface, it follows from (2.9) that the transverse velocity in the outer layer as $x \to 0^-$ is given by

$$\bar{v} = \epsilon^2(\eta F_1' - F_1) + \ldots. \tag{3.32}$$

Note that in the surface boundary layer

$$\bar{v} \to 0 \quad \text{as } \eta \to 0, \qquad \bar{v} \to \epsilon^2 \quad \text{as } \eta \to \infty, \tag{3.33}$$

for $x < 0$. In the outer near wake, $\bar{v}$ is given by (3.23); for fixed $x \gg \Delta_1$, it follows from (3.19) that $\Delta_n \sim \epsilon\kappa x$ as $Re \to \infty$ and the leading-order form of (3.23) is

$$\bar{v} = \epsilon^2(\eta F_1' - F_1 - 1). \tag{3.34}$$

In the outer near wake,

$$\bar{v} \to -\epsilon^2 \quad \text{as } \eta \to 0, \qquad \bar{v} \to 0 \quad \text{as } \eta \to \infty. \tag{3.35}$$

As shown schematically in figure 3, (3.32) and (3.34) do not match as $|x| \to 0$ and an adjustment region of streamwise extent Δ_s is required to resolve the non-uniformity.

The leading-order boundary-layer and near-wake flows give rise to second-order velocity perturbations in the inviscid flow region which will be denoted by u_1 and

v_1. The complex velocity perturbation $u_1 - iv_1$ may be determined using thin-airfoil theory in terms of the distribution of the transverse velocity along $y = 0$, viz.

$$u_1 - iv_1 = \frac{1}{\pi}\int_{-\infty}^{\infty} \frac{v_1(\xi, 0)}{z-\xi} d\xi. \tag{3.36}$$

Here z is the complex variable $z = x + iy$. The variation of $v_1(x, 0)$ is given by

$$v_1(x,0) = \begin{cases} 0 & \text{for } x < x_1, \\ \epsilon^2 & \text{for } x_1 < x < 0, \\ 0 & \text{for } x > 0. \end{cases} \tag{3.37}$$

where x_1 denotes the effective starting location of the turbulent boundary-layer flow. The contributions due to the laminar and transitional boundary layers for $-1 < x < x_1$ are $o(\epsilon^2)$ and are formally negligible with respect to the $O(\epsilon^2)$ velocity associated with the turbulent boundary-layer flow. For the surface boundary layer, it follows by differentiation of (2.15) that $u'_* = O(u_*^2)$; hence the variation in $v_1(x, 0)$ is slow with respect to x and can be represented to leading order as ϵ^2 over the entire portion of the turbulent boundary layer.

Substitution of (3.37) into (3.36) leads to the following solutions for u_1 and v_1:

$$u_1 = -\frac{\epsilon^2}{2\pi}\log(x^2+y^2) + \frac{\epsilon^2}{2\pi}\log((x-x_1)^2+y^2), \tag{3.38}$$

$$v_1 = \frac{\epsilon^2}{\pi}\arg z - \frac{\epsilon^2}{\pi}\arg(z-x_1). \tag{3.39}$$

Thus for $y \to 0$, the perturbation velocities are small but become appreciable near $x = 0$ or near $x = x_1$.

An adjustment region with streamwise extent $\Delta_s = O(\Delta_0)$ leads to a self-consistent description of the flow at the trailing edge and a resolution of the non-uniformity in transverse velocity. With the streamwise coordinate in this region formally defined by $\tilde{x} = x/\Delta_0$, the dependent variables are written in terms of expansions about the surface boundary-layer and mainstream values, viz.

$$\bar{u} = 1 + \epsilon F_1'(\eta) - \frac{\epsilon^2}{\pi}\log\Delta_0 - \frac{\epsilon^2}{2\pi}\log(\tilde{x}^2+\eta^2) + \epsilon^2\tilde{u}_2(\tilde{x},\eta) + \ldots, \tag{3.40}$$

$$\bar{v} = \frac{\epsilon^2}{\pi}\Theta(\tilde{x},\eta) + \epsilon^2\tilde{v}_2(\tilde{x},\eta) + \ldots, \tag{3.41}$$

and

$$\bar{p} = p_0 + \frac{\epsilon^2}{\pi}\log\Delta_0 + \frac{\epsilon^2}{2\pi}\log(\tilde{x}^2+\eta^2) + \epsilon^2\tilde{p}_2(\tilde{x},\eta) + \ldots. \tag{3.42}$$

In (3.40)–(3.42), $\tilde{u}_2$, $\tilde{v}_2$, and $\tilde{p}_2$ are perturbation functions to be determined and $\Theta(\tilde{x}, \eta)$ is the polar angle measured with respect to the positive x-axis, viz.

$$\Theta(\tilde{x},\eta) = \begin{cases} \arctan\left(\dfrac{\eta}{\tilde{x}}\right), & \tilde{x} > 0, \\ \pi + \arctan\left(\dfrac{\eta}{\tilde{x}}\right), & \tilde{x} < 0. \end{cases} \tag{3.43}$$

In the adjustment region, the Reynolds stress distributions are assumed to be independent of $\tilde{x}$ to leading order, and to have distributions corresponding to those in the boundary layer immediately upstream of the trailing edge (see, for example, the discussion by Melnik 1980). Accordingly, the Reynolds stress terms in the adjustment region are written

$$-\overline{u'^2} = \epsilon^2 Q(\eta) + \ldots, \quad -\overline{v'^2} = \epsilon^2 R(\eta) + \ldots, \quad -\overline{u'v'} = \epsilon^2 \Sigma_1(\eta) + \ldots, \tag{3.44}$$

where the functions Q, R and Σ_1 are the limiting forms of the Reynolds stress terms as $x \to 0^-$.

Upon substitution of (3.40)–(3.44) into (2.1), the leading-order equations in the adjustment region may be identified as

$$\frac{\partial \tilde{u}_2}{\partial \tilde{x}} + \frac{\partial \tilde{v}_2}{\partial \eta} = 0, \quad \frac{\partial \tilde{u}_2}{\partial \tilde{x}} = -\frac{\partial \tilde{p}_2}{\partial \tilde{x}} - \Sigma_1', \quad \frac{\partial \tilde{v}_2}{\partial \tilde{x}} = -\frac{\partial \tilde{p}_2}{\partial \eta} - R'. \tag{3.45a–c}$$

The pressure $\tilde{p}_2$ may be eliminated from (3.45b,c) and it is easily shown that $\tilde{v}_2$ satisfies

$$\frac{\partial^2 \tilde{v}_2}{\partial \tilde{x}^2} + \frac{\partial^2 \tilde{v}_2}{\partial \eta^2} = -\Sigma_1''. \tag{3.46}$$

The solution for $\tilde{v}_2$ is

$$\tilde{v}_2 = -\Sigma_1(\eta) = \eta F_1' - F_1 - 1, \tag{3.47}$$

and the corresponding solutions for $\tilde{u}_2$ and $\tilde{p}_2$ are

$$\tilde{u}_2 = \tilde{x}\Sigma_1'(\eta) = \tilde{x}\eta F_1'', \quad \tilde{p}_2 = R(\eta). \tag{3.48}$$

The complete solution for the transverse velocity in the adjustment region is

$$\bar{v} = \frac{\epsilon^2}{\pi}\Theta(\tilde{x}, \eta) + \epsilon^2[\eta F_1' - F_1 - 1] + \ldots, \tag{3.49}$$

and it may be seen that $\bar{v}$ varies smoothly in the outer layer in the vicinity of the trailing edge.

4. Discussion

The general asymptotic analysis described in the preceding section shows that the turbulent near wake has a well-defined double structure. The primary effects of the change in boundary conditions at the trailing edge are contained in a thin inner-wake region whose thickness grows linearly (to leading order) with distance from the trailing edge. In the outer layer, the boundary-layer flow evolves downstream of the trailing edge relatively undisturbed by the change in boundary conditions along $y = 0$; the streamwise velocity profile is determined by the outer-layer surface profile and a downward transverse velocity evolves to accommodate the accelerating flow in the inner wake. An outer-layer adjustment region $O(\Delta_0) \times O(\Delta_0)$ is required near the trailing edge in order to resolve a non-uniformity in transverse velocity; the solution for the transverse velocity in this region is essentially a continuation of the local perturbed inviscid flow.

The development of the turbulent near-wake flow is rather different from the laminar near-wake flow originally described by Goldstein (1930). In the laminar case, the near-wake region also exhibits a double structure but the inner-wake thickness grows proportional to $x^{\frac{1}{3}}$, as opposed to linear growth with x in the turbulent case. A more significant difference between the two flow problems concerns the nature of the

outer-wake flow. In the laminar case, the transverse velocity induced by the inner wake dominates the development of the outer wake and leads to important alterations in the streamwise profile; in the turbulent case, the streamwise profile in the outer layer is relatively unaffected by the developing flow in the inner near wake. The structure of the flow near the trailing edge is also rather different; in laminar flow, the strong displacement effect of the inner wake produces a relatively significant modification of the mainstream pressure distribution near the trailing edge. The inviscid–viscous interaction is described by the 'triple-deck' analysis of Messiter (1970) and Stewartson (1969) which shows that the effects of the trailing edge extend over distances $O(Re^{-\frac{3}{8}})$, well beyond the $O(Re^{-\frac{1}{2}})$ boundary-layer thickness. For a turbulent trailing-edge flow, the non-uniformity in $\bar{v}$ is resolved in a square adjustment region confined within the boundary layer. Significant displacement effects are evidently confined to a region that is exponentially small and $O(\Delta_1)$ at the trailing edge, through which the surface wall layer responds to the change in boundary conditions at the trailing edge.

An important objective of the present analysis was to obtain general results and here the leading-order analysis has been completed without adopting a specific turbulence model. A considerable amount of information may be obtained from the general theory. For example, it follows from (3.3), (3.8) and (3.13) that along the wake centreline, the streamwise velocity may be written in the form

$$u_{\mathrm{CL}}(x; Re) = 1+\epsilon\left[\frac{1}{\kappa}\log\left(\frac{\Delta_n}{\Delta_0}\right)+a_0\right]. \tag{4.1}$$

Here a_0 is a constant equal to the value of f''_{w} at the wake centreline ($z = 0$). To determine a_0, a turbulence model for σ_{w} must be specified; the solution of (3.14) may then be obtained subject to conditions (3.15) and (3.16). It should be emphasized however that all other quantities and scales in (4.1) are known from the scales and constants that characterize the surface boundary layer at the trailing edge; the influence of turbulence model in (4.1) is therefore relatively weak. Expressions equivalent to (4.1) have been obtained in previous analytical treatments of the near wake; as discussed in §1, these works either have invoked a specific turbulence model at the outset (Alber 1980; Prabhu & Patel 1982) or have employed informal analytical means (Robinson 1969). In addition, an empirical relation similar to (4.1) has been suggested previously by Andreopoulos & Bradshaw (1980).

Another general result concerns the behaviour of the Reynolds stress along the centreline. It is easily shown using (3.1), (3.5) and (3.14) that

$$-\frac{\partial\overline{u'v'}}{\partial y}\bigg|_{y=0} = \frac{\epsilon^2}{\Delta_n}. \tag{4.2}$$

In the limit of infinite Re, $\Delta_n \sim \epsilon\kappa x$ at finite x (cf. (3.19)) and thus (4.2) predicts that the Reynolds stress gradient decays on the centreline according to $\epsilon/\kappa x$ to leading order. Strong support for this behaviour is evident in comparisons with experimental data given subsequently in §6. Finally, a displacement thickness δ^* may be defined for the surface boundary layer or the wake by

$$\delta^* = \int_0^\infty (1-\bar{u})\,dy. \tag{4.3}$$

It may be shown using (3.3), (3.18) and (3.22) that the leading-order form for δ^* near the trailing edge is given by

$$\delta^*(x) = \delta^*(0) - \frac{\epsilon \Delta_n}{\kappa} + \epsilon^2 x + \ldots, \tag{4.4}$$

where $\delta^*(0)$ is the displacement thickness of the surface boundary layer evaluated at the trailing edge (as $x \to 0^-$).

In order to produce profiles for velocity and Reynolds stress in the wake, it is necessary to specify a turbulence model. This is considered in the next section, and in §6 a direct comparison of (4.1) and experimental data will be made.

5. Turbulence models

5.1. *Introduction*

To obtain explicit velocity fields in both the wake and surface boundary layer, it is necessary to adopt specific turbulence models. In conventional closure schemes, the Reynolds stress $\overline{u'v'}$ is assumed to be related to the mean velocity field in some universal way. In the present study, the turbulence models employed are tailored to reflect the features of individual flow regions in the simplest possible manner. This approach follows recent trends in turbulence research wherein the concept of a universal turbulence model is abandoned in favour of 'zonal models' that represent a specific geometrical or flow effect locally (cf. Kline 1982). Indeed, the sharp-trailing-edge problem provides an example for which it does not appear possible to extend a surface boundary-layer turbulence model without modification into the wake region in a rational way.

Ideally, zonal turbulence models should reflect the nature of the averaged dynamics of the time-dependent turbulent flow. Recently, Walker, Scharnhorst & Weigand (1986) have described a model for the surface wall layer which reflects the experimentally observed coherent structure of the near-wall flow; this model was used in the present investigation. The dynamics of the Reynolds-stress-producing events in the surface outer layer, as well as the near wake, are not well understood and in these regions an algebraic eddy viscosity model of the form

$$-\overline{u'v'} = \epsilon_m^*(x, y) \frac{\partial \bar{u}}{\partial y} \tag{5.1}$$

was used, where ϵ_m^* is a specified function. It is worth remarking that a physical basis for (5.1) has never been established and that it should be regarded as an *ad hoc* model which is capable of describing mean turbulent flow behaviour in certain situations.

5.2. *Surface boundary-layer models*

It is well known from experimental observation over several decades that the time-dependent flow in the wall layer of a turbulent boundary layer exhibits a remarkable degree of coherent structure. The wall-layer flow is cyclical in character in which relatively long quiescent periods are disrupted by violent bursting phenomena; in the bursting process, wall-layer fluid is ejected into the outer region of the boundary layer. The process may be viewed as a brief but strong viscous–inviscid interaction between the wall layer and the outer layer. It follows from (2.12) that if the Reynolds stress function is known, the profile U^+ may be obtained by integration and vice

versa. Walker *et al.* (1986, 1988) have argued that the principal contributions to U^+ are made during the relatively long quiescent periods (see also Beljaars, Krishan Prasad & de Vries 1981), while contributions to $\overline{u'v'}$ are made intermittently at isolated spanwise and streamwise locations during the bursting process; these authors then consider possible time-dependent solutions during a typical quiescent period in the wall layer. The detailed analysis (Walker *et al.* 1986) is complex but a time average of the results yields a relatively simple analytical expression for the mean velocity profile in the wall layer which has the functional form

$$U^+ = U^+(y^+; \kappa, S). \tag{5.2}$$

Here κ is the von Kármán constant and $S = (T_B^+)^{\frac{1}{2}}$, where T_B^+ is the average period between bursts (in wall-layer units). This wall-layer profile model has been compared extensively with experimental data by Scharnhorst, Walker & Abbott (1977) and Yuhas & Walker (1982) who found the model gives a very close representation of measured profile data. For a constant-pressure turbulent boundary layer, values of $\kappa = 0.41$ and $S = 10.5$ yield excellent comparisons with experimental measurements; these values also produce the conventional value of the constant $C_1 = 5.0$ in the law-of-the-wall equation (2.14). In addition, the corresponding value of $T_B^+ = 110.2$ compares favourably with direct experimental measurements of the burst period.

In specifying a model for closure of the outer-layer equation (2.8), it is convenient to define a scaled eddy viscosity function according to

$$\epsilon_m = \frac{\epsilon_m^*}{u_* \Delta_0} = \frac{\epsilon_m^*}{\delta^*}, \tag{5.3}$$

using the outer scale defined in (2.7). It follows from (2.5) that the outer-layer Reynolds stress function is given by

$$\Sigma_1(\eta) = \epsilon_m(\eta) F_1''(\eta). \tag{5.4}$$

The eddy viscosity function is constrained to behave in specific ways. First, to ensure the logarithmic behaviour in the velocity profile for small η indicated by (2.13), $\epsilon_m \sim \kappa\eta$ as $\eta \to 0$. A linear eddy viscosity throughout the outer layer is not acceptable since the solution of (2.18) must decay exponentially for large η; it follows that ϵ_m must approach a constant (at most) as $\eta \to \infty$. The simplest eddy viscosity distribution having these characteristics is the ramp function

$$\epsilon_m = \begin{cases} K & \text{for } \eta \leqslant \eta_1 = K/\kappa, \\ \kappa\eta & \text{for } \eta < \eta_1. \end{cases} \tag{5.5}$$

Here K is a constant that is usually taken to be about 0.016 (Mellor & Gibson 1966; Cebeci & Smith 1974). Note that the formula (5.5) has a discontinuity in slope at $\eta = \eta_1$; it is possible to construct model functions for ϵ_m that have a smooth variation everywhere (Yuhas & Walker 1982) but one attractive feature of (5.5) is that solutions of (2.18) may be obtained in closed form, viz.

$$F_1'(\eta) = \begin{cases} -\mathrm{e}^{-K/2\kappa^2}\left(\dfrac{\pi}{2K}\right)^{\frac{1}{2}} \operatorname{erfc}\left[\dfrac{\eta}{(2K)^{\frac{1}{2}}}\right], & \text{for } \eta \geqslant \eta_1, \\ -\dfrac{1}{\kappa}E_1\left(\dfrac{\eta}{\kappa}\right) + C_0 - \dfrac{1}{\kappa}[\gamma_0 - \log\kappa], & \text{for } \eta < \eta_1. \end{cases} \tag{5.6}$$

Here E_1 is the exponential integral (Abramowitz & Stegun 1964) and γ_0 is Euler's constant. The outer-layer Reynolds stress distribution is easily obtained from (5.4), and in (5.6) the outer-layer log-law constant is given by

$$C_0 = \frac{1}{\kappa}\left[\gamma_0 - \log\kappa + E_1\left(\frac{K}{\kappa^2}\right)\right] - \mathrm{e}^{-K/2\kappa^2}\left(\frac{\pi}{2\kappa}\right)^{\frac{1}{2}} \operatorname{erfc}\left[\left(\frac{K}{2\kappa^2}\right)^{\frac{1}{2}}\right], \tag{5.7}$$

It may be observed that the outer-layer solution contains the two constants, κ and K. For the conventional values of $\kappa = 0.41$ and $K = 0.016$, equation (5.7) yields $C_0 = 0.97936$.

5.3. *Near-wake models*

In §3.3, it was shown that the solution in the outer near wake is a continuation of the surface outer layer and consequently the Reynolds stress distribution is given by (5.4)–(5.6). For the inner near wake, it may be confirmed using (3.3), (3.5) and (5.1) that the eddy viscosity ϵ_m^* and inner-wake stress functions must have the form

$$\epsilon_m^* = \epsilon \Delta_n(x; Re)\, \epsilon_{mw}(z), \quad \sigma_w = \epsilon_{mw}(z) f_w''(z). \tag{5.8}$$

Here ϵ_{mw} is a scaled eddy viscosity function for the inner-wake region which is to be selected subject to two constraints. First, $\epsilon_{mw} \sim \kappa z$ as $z \to \infty$ in order to match the outer-near-wake distribution given by (5.5). The second constraint is obtained by substituting (5.8) into (3.17) and expanding f_w in a Taylor series about the wake centreline $z = 0$ where $f_w(0) = f_w''(0) = 0$; it is easily shown that ϵ_{mw} cannot vanish at the wake centreline. The simplest function that satisfies these constraints is the ramp function

$$\epsilon_{mw} = \begin{cases} \kappa z & \text{for } z \geqslant \alpha, \\ \kappa\alpha & \text{for } z < \alpha. \end{cases} \tag{5.9}$$

Here α is a model constant to be determined subsequently from comparisons with experimental data.

The eddy viscosity model in (5.9) has a discontinuity in slope at $z = \alpha$; in principle, it is possible to develop a model function that has a smooth variation throughout the inner wake but one advantage of (5.9) is that a solution of (3.14) is readily obtained in closed form. The solution for the inner-wake velocity perturbation is

$$f_w'(z) = \begin{cases} \dfrac{1}{\kappa}[\log z - a_1 E_1(z)] + C_0, & z \geqslant \alpha. \\ \dfrac{2}{\kappa} D_1\left(\dfrac{z}{(2\alpha)^{\frac{1}{2}}}\right) + C_0 + \dfrac{1}{\kappa} a_2, & z \leqslant \alpha. \end{cases} \tag{5.10}$$

Here D_1 is the integral of Dawson's integral $D_0(x)$ (Abramowitz & Stegun 1964), viz.

$$D_0(x) = \mathrm{e}^{-x^2} \int_0^x \mathrm{e}^{t^2}\, \mathrm{d}t, \quad D_1(x) = \int_0^x D_0(t)\, \mathrm{d}t. \tag{5.11}$$

In addition, the constants a_1 and a_2 in (5.10) are given by

$$a_1 = \mathrm{e}^{\alpha}[1 - (2\alpha)^{\frac{1}{2}} D_0((\tfrac{1}{2}\alpha)^{\frac{1}{2}})], \quad a_2 = \log\alpha - a_1 E_1(\alpha) - 2D_1((\tfrac{1}{2}\alpha)^{\frac{1}{2}}). \tag{5.12}$$

The inner-wake Reynolds stress function is easily obtained from (5.8) and (5.10) and is given by

$$\sigma_w(z) = \begin{cases} 1 - a_1 \mathrm{e}^{-z}, & z \geqslant \alpha, \\ (2\alpha)^{\frac{1}{2}} D_0[z/(2\alpha)^{\frac{1}{2}}], & z < \alpha. \end{cases} \tag{5.13}$$

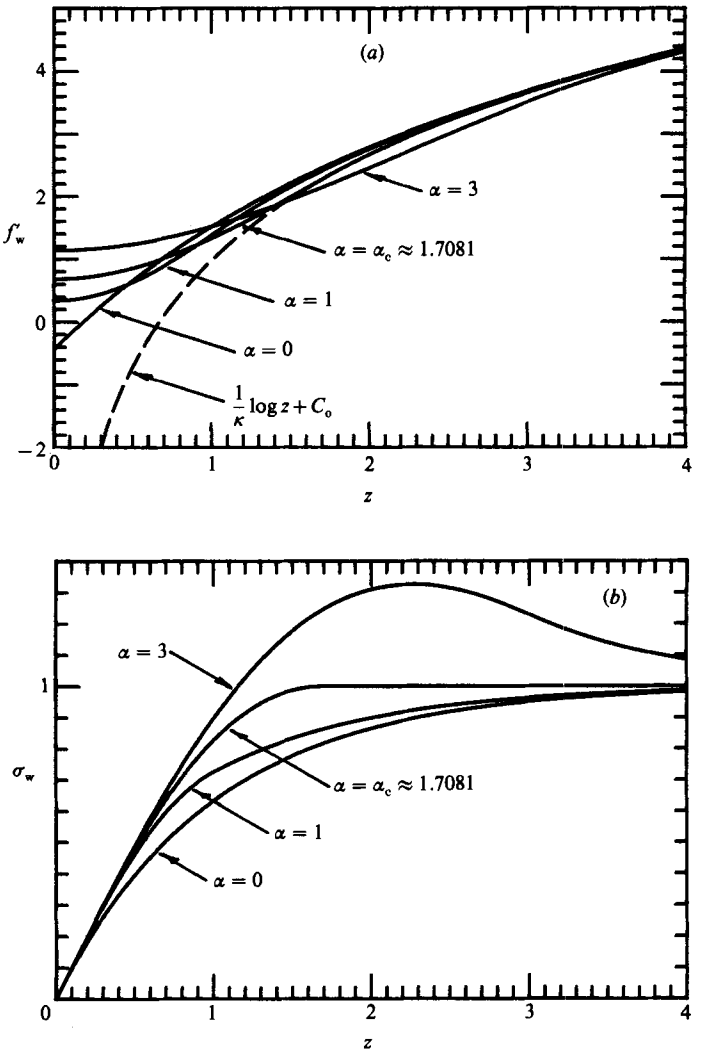

FIGURE 4. Inner-wake profiles obtained with model (5.9) for various α (with $\kappa = 0.41$ and $C_0 = 0.979$). (*a*) Inner-wake velocity profiles. (*b*) Inner-wake Reynolds stress profiles.

The velocity and Reynolds stress distributions in the inner near wake are given by (5.10)–(5.12) which contain the von Kármán constant κ and the single inner-wake modelling constant α; there is also an implicit dependence on K through the outer 'log-law' constant C_0 (cf. (5.7)). A value of the constant α will be obtained in §6 through direct comparisons with experimental data. It is worth discussing here the general features of the inner-wake solution for various values of α.

In figure 4(*a*), a series of inner-wake velocity profiles are plotted for various values of α (with $\kappa = 0.41$ and $C_0 = 0.97936$). The logarithmic curve in this figure corresponds to the asymptotic behaviour for large z and it may be observed that all profiles quickly approach the asymptotic condition. The curve labelled $\alpha = 0$ is a limiting case which, from (5.9), corresponds to a linear eddy viscosity variation across the entire inner wake; this model was adopted by Alber (1980) but it may be observed that the velocity profile has a non-zero slope at the wake centreline which is

not physically realistic. All positive values of α lead to velocity profiles that satisfy the symmetry condition $f''_{\mathrm{w}}(0) = 0$ at the centreline.

In figure 4(*b*) the inner-wake Reynolds stress profiles given by (5.13) are plotted for several values of α; it is evident that the nature of the inner-wake Reynolds stress distribution changes at a certain critical value $\alpha = \alpha_{\mathrm{c}}$. For $\alpha > \alpha_{\mathrm{c}}$, a bulge appears in the Reynolds stress profile and this does not seem acceptable on physical grounds. The Dawson integral $D_0(x)$ has a maximum at $x = x_{\mathrm{c}} = 0.92414$ and if $(\frac{1}{2}\alpha)^{\frac{1}{2}} > x_{\mathrm{c}}$, the maximum in D_0 will be contained in the region $z < \alpha$. Consequently, in order to avoid a bulge in the σ_{w} profile, it would appear that acceptable values of α must be in the range $\alpha < \alpha_{\mathrm{c}}$, where $\alpha_{\mathrm{c}} = 2x_{\mathrm{c}}^2 = 1.7081$.

The eddy viscosity distributions adopted here for the near-wake region may be consolidated into a composite function. In terms of the outer-wake coordinate η, the eddy viscosity distribution at any streamwise position may be written

$$\epsilon_m = \begin{cases} K, & \eta \geqslant \eta_1 = K/\kappa, \\ \kappa\eta, & \eta_{\mathrm{w}} < \eta < \eta_1, \\ \kappa\alpha\Delta_n/\Delta_0, & \eta \leqslant \eta_{\mathrm{w}}, \end{cases} \tag{5.14}$$

where η_{w} is defined by

$$\eta_{\mathrm{w}}(x; Re) = \alpha \frac{\Delta_n(x; Re)}{\Delta_0(Re)}. \tag{5.15}$$

The composite eddy viscosity model is shown schematically in figure 5. At the trailing edge, the eddy viscosity distribution has the simple ramp form associated with the conventional surface outer-layer model. In the near wake, the linear behaviour $\epsilon_m = \kappa\eta$ occurs between $\eta = \eta_1 = K/\kappa$ and $\eta = \eta_{\mathrm{w}}$, which is the curve defined by $z = \alpha$; below $\eta = \eta_{\mathrm{w}}$ the eddy viscosity is constant all the way to the wake centreline. As the inner wake spreads, Δ_n increases, which leads to an increase in η_{w} as well as the centreline eddy viscosity, which has the value $\kappa\alpha\Delta_n/\Delta_0$. Eventually, the centreline value grows to the outer-wake value K. At this stage, the eddy viscosity distribution is constant across the wake and the present inner-wake model ceases to be appropriate; note that this occurs at the streamwise location x_K defined by

$$\Delta_n(x_K; Re) = \frac{K}{\kappa\alpha}\Delta_0(Re). \tag{5.16}$$

Downstream of the position x_K, a suitable turbulence model involves an eddy viscosity distribution that is uniform across the wake. The development of the small-defect wake at large distances from the trailing edge is well known to be described accurately by such a model (see, for example, Townsend 1976). However, upon comparison with the popularly accepted eddy viscosity value for small-defect far wakes (Tennekes & Lumley 1972; Townsend 1976), it emerges that value for the far-wake flow is nearly three times the outer-layer value $\epsilon_m = K$. Consequently, a transition region, in which the eddy viscosity value grows with distance from the trailing edge, is required to complete the modelling of the wake flow. The modelling and prediction of wake flows in this region will be reported elsewhere. Nevertheless, it should be noted that the present near-wake turbulence model provides the simplest transition between a conventional model in the surface boundary layer and a uniform eddy viscosity distribution in the wake; the eddy viscosity on the centreline increases proportional to the thickness of the inner wake.

It is appropriate here to comment briefly on the recent analysis of Neish & Smith (1988), which employs the eddy viscosity model of Cebeci & Smith (1974) for both the

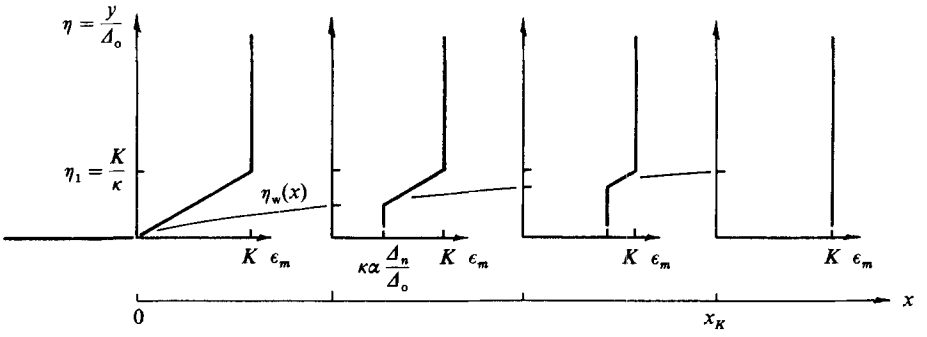

FIGURE 5. Schematic of composite near-wake eddy viscosity distribution $\epsilon_m(x, \eta)$.

surface boundary layer and the wake flow regions. In the outer-layer regions, the Cebeci–Smith scheme is similar to the present model given by (5.5), except that it employs a mixing-length formulation to prescribe the small-η behaviour which is consistent with a logarithmic velocity profile. The validity of the mixing-length portion of the model, which was developed especially for wall-bounded flows, must be regarded as highly doubtful when applied to wake calculations. Indeed, the mixing-length portion of the model produces a cusp in the streamwise velocity profile, which is similar to the case $\alpha = 0$ in figure 4(*a*). Neish & Smith (1988) show that this physically unacceptable behaviour can be resolved in a thin layer $O(Re^{-\frac{3}{5}}\epsilon^{-\frac{1}{5}})$ at the wake centreline that involves a balance of inertia, Reynolds stress, and viscous stress terms. This structure is highly dependent upon the specific turbulence model used. In addition, it should be noted that the Cebeci–Smith model is inconsistent with the well-known description of the small-defect wake that evolves at large distances from the trailing edge.

6. Near-wake flow calculations

6.1. *Introduction*

The objective of this section is twofold. First, the method of determining the modelling constant α that appears in the near-wake eddy viscosity function is described and a single value for practical calculations is selected. Second, the analytical velocity and Reynolds stress profiles obtained in this study are compared directly with experimental data obtained from four modern studies: Chevray & Kovasznay (1969), Pot (1979), Andreopoulos & Bradshaw (1980) and Ramaprian, Patel & Sastry (1981, 1982). (Useful insight into the structure of trailing-edge flows is provided by Haji-Haidari & Smith 1988, who employed a relatively thick plate with a wedge-shaped trailing edge. This type of experimental model is outside the scope of the present work, as discussed by Bogucz 1984.)

There are several features of the experimental configurations that are not taken into account in the present theory, which pertains to an infinitesimally thin flat plate. The experimental studies and the associated issues of concern are discussed in detail by Bogucz (1984); a brief summary of conclusions is given here. The experimental plate models used by Pot (1979) and Ramaprian *et al.* (1982) had trailing-edge thicknesses that are potentially significant; evidence of unsteady separation phenomena at the trailing edge is apparent in the Reynolds stress data reported in these studies. In the experiments of Andreopoulos & Bradshaw (1980),

the tapered trailing edge of the plate model as well as the finite wind-tunnel dimensions combine to produce a significant mainstream pressure gradient at the trailing edge. Finally, in the study of Ramaprian *et al.* (1982), velocity data in the near wake were obtained in three separate measurements (a total head tube and two separate $\times$-wire probe orientations); unfortunately the different methods produce substantially different data at some locations (see Ramaprian *et al.* 1981). The discrepancies are not resolved by the authors and consequently the accuracy of the reported near-wake measurements is uncertain.

The near-wake flow evolves continuously from the profiles in the surface boundary layer immediately upstream of the trailing edge and good predictions of the wake flow can only be expected if the initial surface boundary-layer profile is well represented. A particular velocity profile representation fixes the friction velocity ϵ at the trailing edge, the scales $\Delta_i = (\epsilon Re)^{-1}$ and $\Delta_o = \delta^*/\epsilon$ as well as the von Kármán constant κ and the 'log-law constants' C_i and C_o. If measurements were available at several stations in the surface boundary layer, detailed comparisons with data could be carried out using a boundary-layer prediction method to obtain an accurate representation of the velocity profile as the flow approaches the trailing edge. Unfortunately, sufficient measurements of the surface boundary-layer flow are not reported in the experimental studies. Only Ramaprian *et al.* (1981) report measurements in the upstream boundary layer but these are limited to one streamwise location. In the studies of Chevray & Kovasznay (1969) and Andreopoulos & Bradshaw (1980), the first streamwise location for reported measurements is apparently just downstream of the trailing edge (at $x = 0^+$). The first streamwise data station reported by Pot (1979) is in the wake (at $x = 0.016$).

In the absence of any detailed information concerning the development of the surface boundary layer, the velocity profile at the trailing edge was represented by a composite profile consisting of the wall-layer profile given by (5.2) and the defect profile in (5.6), viz.

$$\bar{u} = 1 + \epsilon\left[F_1'(\eta) + U^+(y^+) - \frac{1}{\kappa}\log\eta - C_o\right]. \tag{6.1}$$

It should be noted that a self-similar, constant-pressure boundary-layer flow at the trailing edge has been assumed in obtaining (6.1) and that these conditions may not be realized at the trailing edge in the cited experiments. It may be inferred that (6.1) implicitly contains the three parameters κ, S and K which, in principle, should assume 'universal' values, at least in a constant-pressure flow. The values $\kappa = 0.41$, $S = 10.5$ (which gives $C_i = 5.0$) and $K = 0.0160$ are conventionally accepted, and provide good representations of experimental data for zero-pressure-gradient boundary layers; these constants uniquely determine the inner and outer logarithmic-law constants C_i and C_o. For each data set, the displacement thickness in the surface boundary layer at the trailing edge was estimated by numerical integration of the raw data at the first data station; using this value of δ^* and with $\Delta_o = \delta^*/u_*$, the value of the friction velocity at the trailing edge ϵ was computed from the match condition (2.15). The values obtained in this manner are listed in table 1(*a*) for each experimental study. Note that the value of ϵ is within the range of estimates 0.037–0.046 given by Chevray & Kovasznay (1969); the value of $\epsilon = 0.0359$ is comparable with the estimate $\epsilon = 0.036$ given by Andreopoulos & Bradshaw (1980).

For two of the experimental data sets, the conventional turbulence model constants did not provide a completely satisfactory representation of the measured data at the trailing edge; this may occur either because pressure gradient effects are

(*a*) Conventional modelling constants ($S = 10.5$, $K = 0.0160$)

Study	Re	δ^*	ϵ	x_K
Chevray & Kovasznay (1969)	6.55×10^5	0.00353	0.0436	0.1771
Andreopoulos & Bradshaw (1980)	6.60×10^6	0.00264	0.0359	0.2185
Pot (1979)	1.20×10^6	0.00350†	0.0410	0.2065
Ramaprian *et al.* (1981)	2.66×10^6	0.00276‡	0.0389	0.1873

(*b*) Optimized modelling constants

Study	S	K	C_i	C_o	ϵ	x_K
Chevray & Kovasznay (1969)	8.10	0.0168	3.478	1.114	0.0470	0.1534
Andreopoulos & Bradshaw (1980)	8.57	0.0121	3.766	0.099	0.0364	0.1873

† Value estimated from experimental measurements at $x = 0.016$.
‡ Value estimated from experimental measurements at $x = -0.0423$.

TABLE 1. Trailing-edge boundary-layer scales and constants

important or because the flow has not entirely achieved self-similarity at the trailing edge. In the absence of information concerning the development of the surface boundary layer, it is not possible to pursue this matter. However, since a good representation of the profile data at the trailing edge is important in relation to the near-wake description, an improvement was sought through optimization of the model constants S and K to produce the best fit to the data at the initial station at the trailing edge, following the approach of Scharnhorst *et al.* (1977) and Yuhas & Walker (1982). The trailing-edge velocity data of Chevray & Kovasznay (1969) is represented extremely well by the profile (6.1) with the conventional constants; direct two-parameter optimization on S and K produced essentially the same results as in table 1(*a*). However, one difficulty is that the reported Reynolds stress data at $x = 0^+$ has a peak at a value that indicates a trailing-edge friction velocity of $\epsilon = 0.0470$ in contrast to the value of 0.0436 in table 1(*a*). A least-squares fit of the reported velocity profile was performed with S and K as parameters, subject to the constraint $\epsilon = 0.0470$; in this manner, it was possible to obtain good representations of both the velocity and Reynolds stress profiles at the trailing-edge and the optimized results are given in table 1(*b*).

An accurate representation of the data at the trailing edge for the experiments of Andreopoulos & Bradshaw (1980) is somewhat more difficult in the context of the present theory. Significant pressure gradient effects evidently were present in the flow near the trailing edge; Patel (1981) and Bogucz (1984) have used independent methods to estimate that the Clauser parameter $\beta = -\delta^* U_e U_e'/u_*^2 \approx 0.5$ for the flow near the trailing edge. In an attempt to obtain an improved representation of the reported data, the parameters S and K were varied to produce an optimal least-squares fit of the velocity data at the trailing edge and the results are given in table 1(*b*). Note that the data used for this purpose correspond to those reported by Andreopoulos in Kline, Cantwell & Lilley (1981).

6.2. *Evaluation of the inner-wake eddy viscosity constant*

For a given representation of the surface boundary-layer profile at the trailing edge, the near-wake solution is completely determined except for the value of the inner-

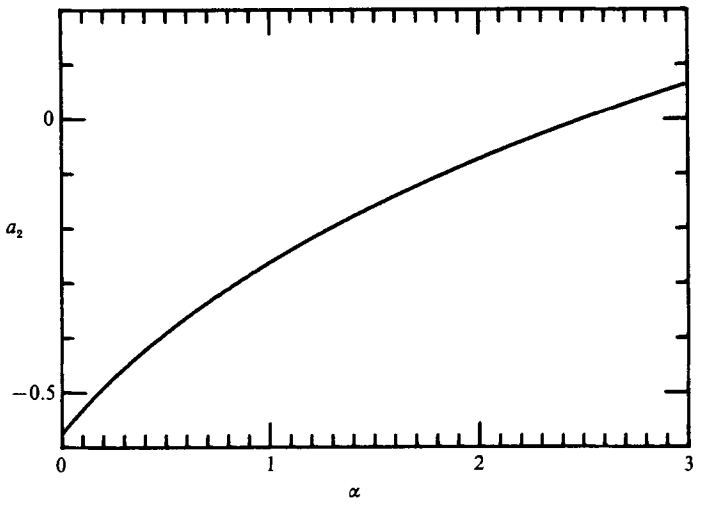

FIGURE 6. Inner-wake model constant a_2.

region eddy viscosity constant α in (5.9). A means of determining a value for α is to make a comparison with experimental data along the centreline. It follows from (3.3) and (3.8) that the predicted centreline velocity (in defect form) behaves according to

$$u_{\mathrm{CL_{def}}}(x) \equiv \frac{u_{\mathrm{CL}}(x)-1}{\epsilon} = \frac{1}{\kappa}\log\frac{\Delta_n}{\Delta_0}+a_0. \tag{6.2}$$

In the context of the general asymptotic analysis of §3, a_0 is a constant that can be determined by direct comparison with experimental data. For the specific inner-wake turbulence model described by (5.1), (5.8) and (5.9), the value of a_0 follows from (5.10) and is

$$a_0 = C_0+\frac{1}{\kappa}a_2(\alpha). \tag{6.3}$$

Here a_2 is the function of the modelling constant α defined in (5.12); its variation with α is shown in figure 6. Note that for a given velocity profile at the trailing edge, a_0 depends only on α.

Using near-wake centreline velocity data from each experimental study, the value of a_0 in (6.2) was systematically varied to produce the best fit to the data in the least-squares sense. The data used in this process were restricted to the range $500\Delta_i < x < 0.15\ \Delta_0/\epsilon$ to avoid effects of the $O(\Delta_i)$ wall-layer adjustment region for small x and the influence of deviations from the near-wake similarity solution for larger values of x. The values of a_0, and the corresponding values of a_2 and α, determined by this procedure are given in table 2 for each set of trailing-edge profile constants listed in table 1. Note that for the data of Ramaprian *et al.* (1981), three entries are listed, corresponding to the measurements taken with a total-head tube and a $\times$-wire as well as an arithmetic mean; centreline data that were used for this purpose were restricted to data stations where both types of measurements were taken. When it is considered that a deviation of 0.1 in a_0 represents a change in centreline velocity of 0.1ϵ (or about 0.6% for typical values), it may be inferred that the values of a_0 are in good agreement between the different experiments.

There are two possible approaches for determining a value of α for all subsequent predictions of velocity and Reynolds stress profiles in the near wake and these are:

(*a*) Conventional surface boundary-layer constants

Study	a_0	a_2	α	Comments
Chevray & Kovasznay (1969)	0.0604	−0.3768	0.5534	
Andreopoulos & Bradshaw (1980)	0.2429	−0.3020	0.8340	
Pot (1979)	0.0715	−0.3722	0.5692	
Ramaprian *et al.* (1981)	0.5798	−0.1638	1.4772	Head-tube data
	−0.0423	−0.4197	0.4114	×-wire data
	0.2678	−0.2918	0.8758	Averaged data

(*b*) Optimized surface boundary-layer constants

Study	a_0	a_2	α
Chevray & Kovasznay (1969)	0.2279	−0.3632	0.6011
Andreopoulos & Bradshaw (1980)	0.3027	0.0836	3.1632

TABLE 2. Inner-wake eddy viscosity α determined by least-squares fit of equation (6.2)

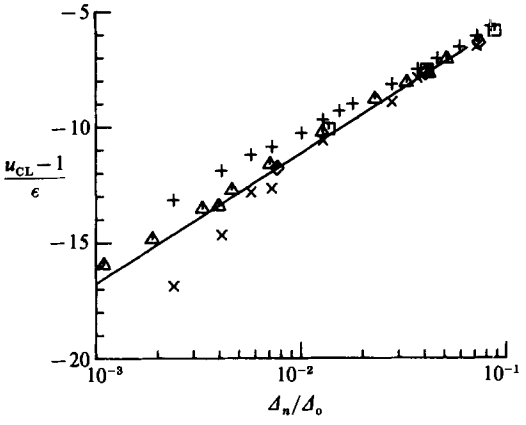

FIGURE 7. Defect centreline velocity: □, Chevray & Kovasznay (1969); △, Andreopoulos & Bradshaw (1980); ◇, Pot (1979); +, Ramaprian *et al.* (1981) head-tube data; ×, Ramaprian *et al.* (1981) ×-wire data; ——, equation (6.2) with $a_0 = 0.0927$.

(1) regard a_0 as a universal value and determine α from (6.3) for each flow; or (2) regard α as a universal constant and compute a_0 from (6.3) for each case. For the set of surface boundary-layer constants normally associated with constant-pressure flows ($S = 10$, $K = 0.016$), the values of $a_0 = 0.1$ and $\alpha = 0.6$ are judged representative of the values listed in table 2. The results for the two sets of optimized trailing-edge constants are not conclusive; the results for the data of Chevray & Kovasznay (1969) tend to support the idea of a universal value of α while the data of Andreopoulos & Bradshaw (1980) tend to support a fixed value of a_0. However, the data of Andreopoulos & Bradshaw (1980) are thought to contain pressure gradient effects that are not accounted for in the present theory and no definitive recommendation is possible at this stage for such flows. For surface boundary-layer flows which may be adequately predicted using the conventional constants, the representative value of $\alpha = 0.6$ is recommended and this produces values of

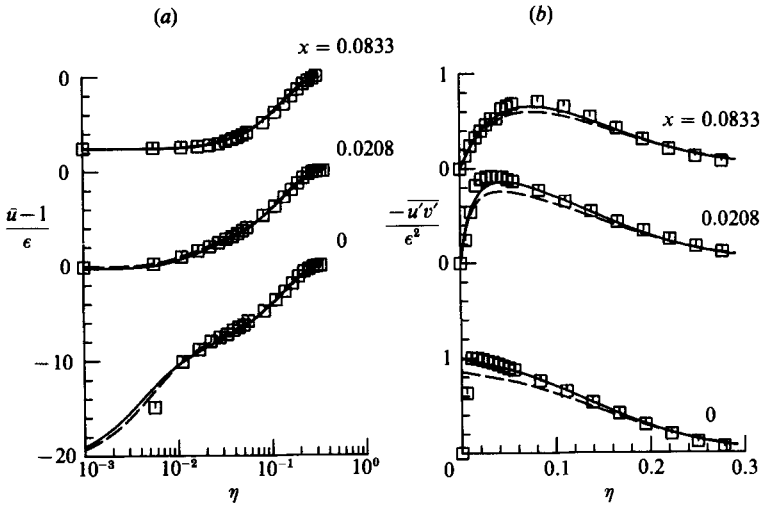

FIGURE 8. Comparison of near-wake predictions with experimental measurements of Chevray & Kovasznay (1969); (*a*) Velocity-defect profiles; (*b*) Reynolds stress profiles (– – –, conventional surface boundary-layer constants; ——, optimized surface boundary-layer constants).

$a_2 = -0.3635$ and $a_0 = 0.09273$. This value of α (along with the conventional set of surface boundary-layer constants) will be shown subsequently to provide very good representations of near-wake experimental data, including the measurements of Andreopoulos & Bradshaw (1980).

The defect centreline velocity given by (6.2) with $a_0 = 0.09273$ is plotted as a function of $\log(\Delta_n/\Delta_0)$ and compared with measured data in figure 7. Note that the data reported by Ramaprian *et al.* (1981) using both total head and ×-wire probes are included; the former measurements progressively diverge from the other data for decreasing x which raises questions about the accuracy of the total-head tube data. Apart from one set of data, the variation in centreline velocity data predicted by (6.2) is strongly supported by the measurements.

6.3. *Profile data comparisons*

In §5.3, analytical functions were obtained which describe the velocity profile and Reynolds stress development throughout the near-wake region; in this section, these profiles are compared directly with experimental profile data. At the outset, it is important to delineate the streamwise range of validity of the present solutions. When $x = O(\Delta_1)$ the present near-wake description is not uniformly valid. For practical purposes, the present inner-wake solutions may be used for x greater than a few hundred multiples of Δ_1; note that $x = 500\Delta_1$, for example, is a rather small distance from the trailing edge and that very few experimental measurements have been taken in this range. The largest value of x for which the present solutions apply is at $x = x_K$; at this location (which is given by (5.16) and is tabulated in table 1), the inner-wake eddy viscosity model becomes uniform across the entire wake.

A composite expansion for the near-wake velocity profile may be written as

$$\bar{u} = u_c(x; Re) + \epsilon\left[f'_w(z) + F'_1(\eta) - \frac{1}{\kappa}\log\eta - C_0\right], \tag{6.4}$$

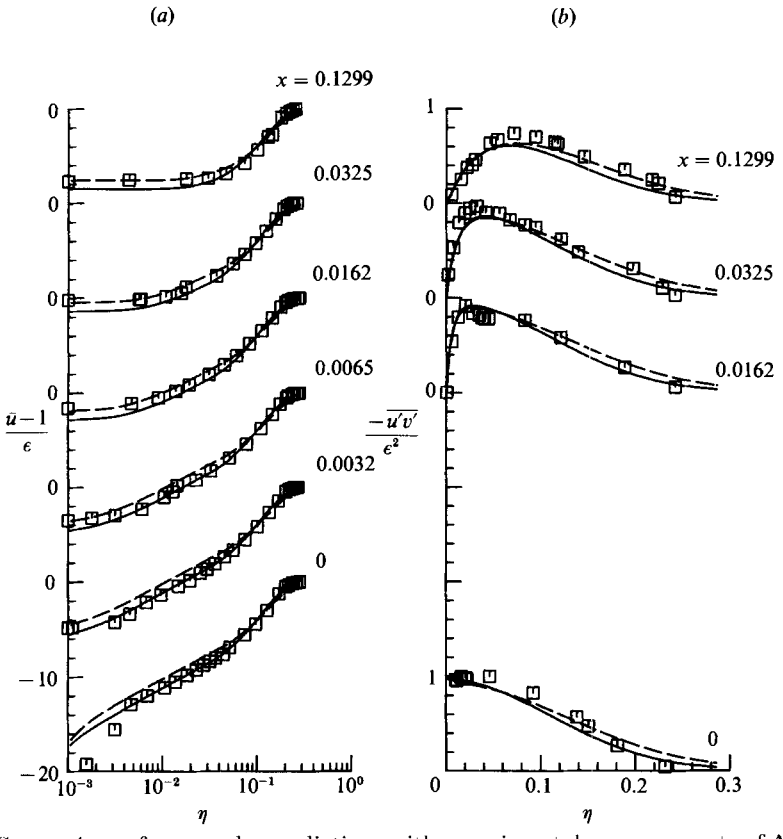

FIGURE 9. Comparison of near-wake predictions with experimental measurements of Andreopoulos & Bradshaw (1980): (*a*) Velocity-defect profiles; (*b*) Reynolds stress profiles (– – –, conventional surface boundary-layer constants; ——, optimized surface boundary-layer constants).

where the functions u_e, F_1' and f_w' are given in (3.8), (5.6) and (5.10) respectively. The composite expansion for the near-wake Reynolds stress is

$$-\overline{u'v'} = \epsilon^2[\sigma_w(z) + \Sigma_1(\eta) - 1], \tag{6.5}$$

where Σ_1 and σ_w are given by (5.4) and (5.13) respectively.

Predicted velocity and Reynolds stress profiles for the two near-wake data stations of Chevray & Kovasznay (1969) are shown in figure 8; the representations for the initial profiles at the trailing edge are also shown. Note that results for both the conventional and optimized set of surface boundary-layer constants are displayed in the figure; the inner-wake eddy viscosity constant $\alpha = 0.6$ was used for both sets of profiles. The analytical profiles agree very favourably with the data for the optimized set of trailing-edge constants and reasonably well for the conventional set. Differences between the results obtained with the two sets of constants are seen to decrease with downstream distance from the trailing edge.

Predicted profiles for the data of Andreopoulos & Bradshaw (1980) are shown in figure 9 for both sets of surface boundary-layer constants and with $\alpha = 0.6$ for both sets of comparisons. It is evident that the initial velocity profile at the trailing edge is not well represented by the conventional set of surface constants. However, the representation of subsequent downstream profiles improves with increasing distance

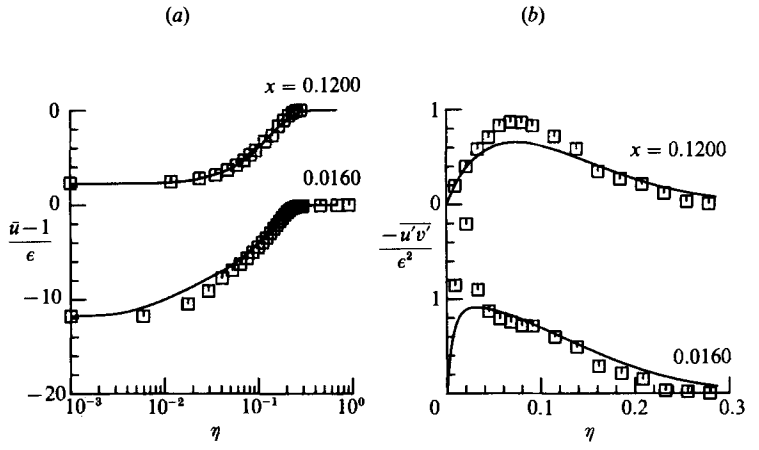

FIGURE 10. Comparison of near-wake predictions with experimental measurements of Pot (1979): (*a*) Velocity-defect profiles; (*b*) Reynolds stress profiles.

from the trailing edge and it is apparent that any pressure gradient effects present in the trailing-edge profile progressively diminish in the near wake. It may be observed that the velocity profiles with the optimized set of surface constants represent the initial velocity profiles very well but then underpredict the velocity at the centreline at subsequent data stations. Note that the value of $\alpha = 0.6$ used in preparing figure 9 is considerably less than the value suggested by the least-squares fit to centreline velocity measurements (see table 2*b*). Nevertheless, the qualitative behaviour of the analytical profiles is sound and the quantitative differences between the predictions and data are small (typically, the differences are $O(\epsilon)$ or smaller, where $\epsilon = 0.036$ in this case).

Figure 10 shows predicted velocity and Reynolds stress profiles for the two near-wake data stations of Pot (1979). Note that the Reynolds stress data at the first station have a maximum value of approximately $1.8\epsilon^2$, which is not well represented by the present theory. This discrepancy is believed to be caused by the relatively thick trailing edge of the experimental model used by Pot; unsteady separation phenomena at a thick trailing edge may be expected to produce a peak in Reynolds stress such as that seen in the data. A similar overshoot in Reynolds stress data has been reported by Ramaprian *et al.* (1982), who also used a model with a relatively thick trailing edge. The reported data indicate that the maximum Reynolds stress values diminish rapidly with distance from the trailing edge, and subsequent downstream stations are well represented by the present theory.

The velocity and Reynolds stress profile predictions shown in figures 8–10 support the analysis described in §3 and the turbulence models proposed in §5. In the context of the general asymptotic analysis, note that the variation of centreline velocity measurements is well represented by the present theory, as shown in figure 7. In addition, the general analysis also predicts the variation of Reynolds stress gradient at the wake centreline, as given by (4.2); figures 8(*b*)–10(*b*) show clearly that this model-independent result is well supported by the measurements. Concerning the accuracy of the simple near-wake eddy viscosity models proposed here, it should be noted that the predicted Reynolds stress profiles shown in figures 8(*b*)–10(*b*) are much more accurate in the near-wake region than reported results (Ramaprian *et al.* 1981) for fully numerical calculations using more complicated one- and two-equation turbulence models.

7. Summary

A rational description of the symmetric flow in the near wake of a flat plate with a sharp trailing edge has been obtained using the method of matched expansions in the limit $Re \to \infty$. A number of fundamental and general results have been obtained without recourse to a specific turbulence model. The turbulent near wake was found to have a double structure consisting of a thin inner-wake region near the wake centreline and a thick outer wake. The flow structure has some superficial similarities to the laminar trailing-edge problem but the mechanics of the turbulent flow problem are substantially different. The primary effects of the change in boundary conditions at the trailing edge are contained in the inner wake; a similarity solution of the governing equation in this region shows that, to leading order, the inner wake grows linearly with distance from the trailing edge. In addition, the general similarity solution shows that the centreline velocity varies logarithmically with the inner region lengthscale in a manner confirmed by experimental measurements. The outer-wake solution for the streamwise velocity is essentially a continuation of the outer-layer surface boundary-layer profile. The main difference from the surface boundary layer is that transverse flow toward the axis $y = 0$ develops to feed the accelerating flow in the inner wake. An $O(\Delta_0) \times O(\Delta_0)$ adjustment region in the outer layers at the trailing edge is required to accommodate the change in direction of the transverse velocity from the surface boundary layer to the outer wake.

To obtain a solution for the velocity and Reynolds stress profiles in the near-wake region, an algebraic eddy viscosity model was proposed; this model has the simplest possible form that permits the symmetry condition for the streamwise velocity profile to be realized on the wake centreline. In addition, the eddy viscosity model permits a simple transition from a conventional eddy viscosity distribution for surface boundary layers to a uniform eddy viscosity distribution for turbulent flow in the wake. Note that, as a consequence of the self-similar behaviour in the near-wake solution, the portion of the eddy viscosity that is linear gradually disappears (cf. figure 5) as the eddy viscosity reaches a uniform value across the wake; as this occurs, the portion of the streamwise profile containing logarithmic behaviour diminishes. In predictions of several experimental flow situations, the analytical near-wake profiles provided accurate representations of reported measurements. Indeed, the simple algebraic eddy viscosity models proposed here for the near-wake region appear to provide more accurate representations of the flow than those obtained in other studies using more complex one- and two-equation turbulence closures (cf. Ramaprian *et al.* 1981).

This work was supported by the National Science Foundation under grant MEA-8016929. The second author would like to acknowledge the continuing support of the Air Force Office of Scientific Research for the development of surface layer turbulence models.

REFERENCES

Abramowitz, M. & Stegun, I. A. 1964 *Handbook of Mathematical Functions*. US Natl Bur. Stand., Appl. Math. Ser., vol. 55.

Alber, I. E. 1980 The turbulent wake of a thin flat plate. *AIAA J.* **18**, 1044–1051.

Andreopoulos, J. & Bradshaw, P. 1980 Measurements of interacting turbulent shear layers in the near wake of a flat plate. *J. Fluid Mech.* **100**, 639–668.

BELJAARS, A. C. M., KRISHNA PRASAD, K. & DE VRIES, D. A. 1981 A structured model for turbulent exchange in boundary layers. *J. Fluid Mech.* **112**, 33–70.

BOGUCZ, E. A. 1984 Analysis of the turbulent near wake at a sharp trailing edge. Ph.D. dissertation, Lehigh University, Bethlehem, PA.

CEBECI, T. & SMITH, A. M. O. 1974 *Analysis of Turbulent Boundary Layers.* Academic.

CHEVRAY, R. & KOVASZNAY, L. S. G. 1969 Turbulence measurements in the wake of a thin flat plate. *AIAA J.* **7**, 1641–1643.

FENDELL, F. E. 1972 Singular perturbation and turbulent shear flow near walls. *J. Astro. Sci.* **20**, 129–165.

GOLDSTEIN, S. 1930 Concerning some solutions of the boundary layer equations in hydrodynamics. *Proc. Camb. Phil. Soc.* **26**, 3–30.

HAJI-HAIDARI, H. & SMITH, C. R. 1988 Development of the turbulent near wake of a tapered thick flat plate. *J. Fluid Mech.* **189**, 135–163.

KLINE, S. J. 1982 Universal or zonal modeling – the road ahead. In *Proc. 1980–81 AFOSR-HTTM-Stanford Conf. of Complex Turbulent Shear Flows*, vol. II (ed. S. J. Kline, B. J. Cantwell, & G. M. Lilley), pp. 991–1015.

KLINE, S. J., CANTWELL, B. J. & LILLEY, G. M. (eds.) 1981 *Proc. 1980–81 AFOSR-HTTM-Stanford Conf. of Complex Turbulent Shear Flows,* Vol. I. Stanford.

MELLOR, G. L. 1972 The large Reynolds number, asymptotic theory of turbulent boundary layers. *Intl J. Engng Sci.* **10**, 851–873.

MELLOR, G. L. & GIBSON, D. M. 1966 Equilibrium turbulent boundary layers. *J. Fluid Mech.* **10**, 225–253.

MELNIK, R. E. 1980 Turbulent interactions on airfoils at transonic speeds – recent developments. *Proc. NATO AGARD Symp. on Computation of Viscous–Inviscid Flows, Colorado Springs, Paper no. 10.*

MELNIK, R. E. & CHOW, R. 1975 Asymptotic theory of two-dimensional trailing-edge flows. In *Aerodynamic Analysis Requiring Advanced Computers, NASA SP-347.*

MELNIK, R. E., CHOW, R. & MEAD, H. R. 1977 Theory of viscous transonic flow over airfoils at high Reynolds number. *AIAA paper* 77–680.

MELNIK, R. E. & GROSSMAN, B. 1981 On the turbulent viscid–inviscid interaction at a wedge-shaped trailing edge. In *Numerical and Physical Aspects of Aerodynamics Flows* (ed. T. Cebeci). Springer.

MESSITER, A. F. 1970 Boundary layer flow near the trailing edge of a flat plate. *SIAM J. Appl. Math.* **18**, 241–257.

NEISH, A. & SMITH, F. T. 1988 The turbulent boundary layer and wake of an aligned flat plate. *J. Engng Maths* **22**, 15–42.

PATEL, V. C. 1981 Two-dimensional wakes. In *Proc. 1980–81 AFOSR-HTTM-Stanford Conf. of Complex Turbulent Shear Flows*, Vol. I (ed. S. J. Kline, B. J. Cantwell & G. M. Lilley), pp. 340–363. Stanford.

POT, P. J. 1979 Measurements in a 2D wake and in a 2D wake merging into a boundary layer. *Rep. NLR TR* 79063 *U*. National Aerospace Laboratory NLR, Netherlands.

PRABHU, A. & PATEL, V. C. 1982 Analysis of turbulent near wakes. *Iowa Inst. of Hydraulic Research Rep.* 253. University of Iowa, Iowa City.

RAMAPRIAN, B. R., PATEL, V. C. & SASTRY, M. S. 1981 Turbulent wake development behind streamlined bodies. *Iowa Institute of Hydraulic Research Rep.* 231. University of Iowa, Iowa City.

RAMAPRIAN, B. R., PATEL, V. C. & SASTRY, M. S. 1982 The symmetric turbulent wake of a flat plate. *AIAA J.* **20**, 1228–1235.

ROBINSON, J. L. 1969 Similarity solutions in several turbulent shear flows. *Rep.* 1242. National Physical Laboratory, Teddington, UK.

ROTTA, J. C. 1962 Turbulent boundary layers in incompressible flow. *Prog. Aero. Sci.* **2**, 1–219.

SHARNHORST, R. K., WALKER, J. D. A. & ABBOTT, D. E. 1977 Comparisons of theoretical profiles for a two-dimensional time-mean turbulent boundary layer with experimental data. *AFSOR-TR*-77-0877.

SMITH, F. T. 1982 On the high Reynolds number theory of laminar flows. *IMA J. Appl. Maths* **28**, 207–281.

STEWARTSON, K. 1969 On the flow near the trailing edge of a flat plate. *Mathematica* **16**, 106–121.

STEWARTSON, K. 1974 Multistructured boundary layers on flat plates and related bodies. *Adv. Appl. Mech.* **14**, 145–239.

TENNEKES, H. & LUMLEY, J. L. 1972 *A First Course in Turbulence*. MIT Press.

TOWNSEND, A. A. 1965 Self-preserving flow inside a turbulent boundary layer. *J. Fluid Mech.* **22**, 773–797.

TOWNSEND, A. A. 1966 The flow in a turbulent boundary layer after a change in surface roughness. *J. Fluid Mech.*, **26**, 255–266.

TOWNSEND, A. A. 1976 *The Structure of Turbulent Shear Flow*, 2nd edn. Cambridge University Press.

WALKER, J. D. A., ABBOTT, D. E., SCHARNHORST, R. K. & WEIGAND, G. G. 1988 A wall layer model for the velocity profile in turbulent flows. *AIAA J.* (to appear).

WALKER, J. D. A., SCHARNHORST, R. K. & WEIGAND, G. G. 1986 Wall layer models for the calculation of velocity and heat transfer in turbulent boundary layers. *AIAA Paper* 86-0213. Reno, Nevada.

YUHAS, L. J. & WALKER, J. D. A. 1982 An optimization technique for the development of two-dimensional steady turbulent boundary layer models. *AFOSR-TR*-82-0417.